Check for updates

Oxo Clusters Hot Paper

How to cite:
International Edition: doi.org/10.1002/anie.202016522
German Edition: doi.org/10.1002/ange.202016522

Ce^{IV}_{70} Oxosulfate Rings, Frameworks, Supramolecular Assembly, and Redox Activity**

*Ian Colliard and May Nyman**

Abstract: *M^{IV} molecular oxo-clusters (M = Zr, Hf, Ce, Th, U, Np, Pu) are prolific in bottoms-up material design, catalysis, and elucidating reaction pathways in nature and in synthesis. Here we introduce Ce_{70}, a wheel-shaped oxo-cluster, $[Ce^{IV}_{70}(OH)_{36}(O)_{64}(SO_4)_{60}(H_2O)_{10}]^{4-}$. Ce_{70} crystallizes into intricate high pore volume frameworks with divalent transition metals and Ce-monomer linkers. Eight crystal-structures feature four framework types in which the Ce_{70}-rings are linked as propellers, in offset-stacks, in a tartan pattern, and as isolated rings. Small-angle X-ray scattering of Ce_{70} dissolved in butylamine, with and without added cations (Ce^{IV}, alkaline earths, Mn^{II}), shows the metals' differentiating roles in ring linking, leading to supramolecular assemblies. The large acidic pores and abundant terminal sulfates provide ion-exchange behavior, demonstrated with U^{IV} and Nd^{III}. Frameworks featuring $Ce^{III/IV}$-monomer linkers demonstrate both oxidation and reduction. This study opens the door to mixed-metal, highly porous framework catalysts, and new clusters for metal-organic framework design*

Introduction

Metal-oxo clusters are molecular metal oxides in their structure and function. They are both aesthetically fascinating and fundamentally useful in geosciences, environmental science and materials science. For example, they provide a foundation to understand metal oxide dissolution and precipitation in nature and in synthesis.[1] The atomic precision of metal-oxo clusters allows investigation of chemical processes of non-molecular counterparts including surfaces, bulk materials and nanoparticles.[2] They function as single-molecule magnets and catalysts, linked into frameworks or as isolated clusters.[2a,3] Metal-oxo cluster supramolecular assembly creates another level of complexity and emergent properties in fractals, superlattices and nanomaterials.[4]

One of the most widely exploited families of metal-oxo clusters is that comprised of the large, "hard" tetravalent cations that span transition metals (Zr^{IV}, Hf^{IV}), lanthanides (Ce^{IV}) and actinides (Th^{IV}, U^{IV}, Np^{IV}, Pu^{IV}). The most common topology of M^{IV}-oxo clusters is the hexamer (M_6, $[M^{IV}_6(OH,O)_8]$),[5] which structurally resembles the $M^{IV}O_2$ fluorite-type lattice. This molecular oxide fragment has been stabilized and isolated with carboxylate, nitrate, sulfate, and polyoxometalate ligands.[6] Combining rigid bicarboxylate linkers with Zr^{IV}_6 led to the discovery of the metal-organic framework (MOF) known as UiO-66.[5a] This compound and its derivatives comprise an extensive MOF family known for high stability and functionalizabilty, exploited in separations, storage and catalysis.[8] Not suprising, UiO-66 analogues of Hf^{IV},[7] Ce^{IV},[8] Th^{IV},[9] U^{IV},[10] Np^{IV},[5f] and Pu^{IV} [11] have all been discovered.

Beyond the hexamer, larger M^{IV}-oxo clusters are built symmetrically around the M_6 core, and by extension, are larger fragments of the fluorite lattice. The largest is M_{38}, synthesized from Ce^{IV},[12] Pu^{IV},[2c] U^{IV} [13] and Np^{IV}.[14] Cerium-oxo clusters and nanomaterials are of special relevance.[6e,12] Owed to facile Ce^{III}-Ce^{IV} redox behavior and concomitant oxygen transport, ceria nanoparticles are used as automotive redox catalysts, in oxide fuel cells, and as photoactive solar cell materials.[15] Atomically precise cerium-oxo clusters are valuable to understand form-function relationships; and Ce_{10}, Ce_{20}, Ce_{22}, Ce_{24}, Ce_{38} and Ce_{40} have been isolated, some of which have distinct Ce^{III} and Ce^{IV} sites.[6e,12] Farha and co-workers recently demonstrated catalytic activity of Ce_{38}, owed to the high porosity and redox activity of the solid material.[16]

We exploited Ln^{III} and TM^{II} countercations to create a new family of giant U^{IV}-oxo clusters including the U_{84} "superatom" (with Ln^{III}) and U_{70} wheel (with TM^{II}).[4b,17] Following U_{70}, the Zr_{70} analogue was described in multiple frameworks with transition metals, Mg^{2+}, Na^+ and no countercations.[18] This large toroid, with external and internal diameters of approximately 35 and 17 Å respectively, yields pore volumes in its lattices, up to 60%. Additionally, these cluster-frameworks are insoluble in water and mild acid, yet they can be dissolved in short chain amines. The former insolubility along with high porosity enables applications akin to MOFs, as demonstrated for the Ce_{38} framework;[16] but without unstable organic components. The latter provides opportunity to assemble 2-dimensional cluster arrays onto surfaces.

Herein, we introduce the Ce_{70}-sulfate torus, the third member of the M_{70} family, and unveil some distinct differences from the U_{70} and Zr_{70} families. Specifically, the transition metals and Ce-monomers play a more significant role in framework assembly, leading to four different framework types (instead of one type for U_{70}). The roles are also distinguished upon re-dissolution in amine solution (probed by small angle X-ray scattering, SAXS). Second, frameworks featuring Ce-monomer linkers exhibit redox activity, while

[*] I. Colliard, Prof. Dr. M. Nyman
Department of Chemistry, Oregon State University
Corvallis, OR 97331 (USA)
E-mail: may.nyman@oregonstate.edu

[**] A previous version of this manuscript has been deposited on a preprint server (https://doi.org/10.26434/chemrxiv.12933773.v1).

Supporting information and the ORCID identification number(s) for the author(s) of this article can be found under: https://doi.org/10.1002/anie.202016522.

© 2021 Wiley-VCH GmbH

These are not the final page numbers!

acidity of the pores is demonstrated by cation exchange. The Zr_{70} family shows yet again different arrangements,[18] bringing to light that this emerging family of M^{IV}_{70}-rings could rival other families of cluster-based materials and isolated clusters in both structural and functional diversity.

Results and Discussion

Highly-charged metal cations complex water molecules upon dissolution, followed by deprotonation, even in acidic conditions, promoting oligomerization. If uncontrolled, this process leads to metal oxide precipitation. Adding heterometal cations and strongly coordinating oxoanion ligands mediate the fundamental hydrolysis, olation and oxolation reactions that drive oligomerization.[19] Moreover, countercations play primary roles in the assembly of any oligomeric species in the crystallization process.[20]

Combining transition metals with $Ce^{IV}(SO_4)_2$ and heating at 75 °C (see SI for details) promotes assembly of Ce_{70}; fully formulated $[Ce^{IV}(OH)_{36}(O)_{64}(SO_4)_{60}(H_2O)_{10}]^{4-}$, isostructural with prior reported U_{70} (Figure 1 a).[4b,17] Analogous to U_{70}, the Ce_{70} cluster can be viewed as alternating Ce_6 and Ce_1. Four sulfates bridge a Ce_6 and a Ce_1 along the outer rim, and four additional sulfates bridge only Ce_6 units along the inner rim (Figure 1 b). Like isolated M_6-clusters, the ring exhibits O/OH disorder, as determined by bond valence sum (BVS) calculations. Most Ce-centers are 8-coordinate, with the exception of the innermost Ce of the Ce_6 unit that is capped by an additional water molecule. Charge of Ce^{IV} for Ce_{70} was confirmed by BVS, see Table S12 for a representative example amongst the eight structures. Ce–O bond lengths include: $Ce–OH^-/O^{2-} = 2.11–2.67$ Å, $Ce–OH_2 = 2.28$ Å–2.80 Å, and $Ce–OSO_3 = 2.30–2.99$ Å. Oxygens with a BVS around 2.0 were assigned as O^{2-}, those with BVS ≈ 1.0 were assigned as purely OH^-, and those with BVS in between were assigned as mixed OH^-/O^{2-}. There is evidence for mixed oxidation state amongst the Ce-monomers. BVS suggests trivalent, but many of the sites exhibit partial occupancy and ligand disorder, which makes these assignments ambiguous. Moreover, $Ce^{III/IV}$ oxidation is notoriously difficult to assign by BVS.[21] Redox behavior of the Ce-monomers suggest mixed $Ce^{III/IV}$-monomers, and will be discussed later. The acidic pH (see below and SI) support the possibility of reduction of the Ce^{IV}-starting material. Our assessment based on various evidences is these sites are mixed $Ce^{III,IV}$ valence. For the sake of assigning site occupancy and charge-balance, we provide a formula in the manuscript featuring Ce^{IV}-monomers. In Table S1, a more general formula that accounts for possible $Ce^{III/IV}$-monomers is provided. Final refinements to assign site occupancy and charge-balance is consistent with Ce^{IV}, details are provided in the SI.

Addenda sulfates (Figure 1 c,d), along with TM^{II} and Ce-monomers, decorate and bridge the Ce_{70} rings defining different Ce_{70}-frameworks. Individual TM^{II} bonding behaviors and the synthesis conditions leads to four unique architects, summarized in Figure 2. Based on arrangement of the Ce_{70}-rings, these are dubbed 1) propeller framework, 2) standard offset-stacking, 3) tartan, and 4) isolated rings. The

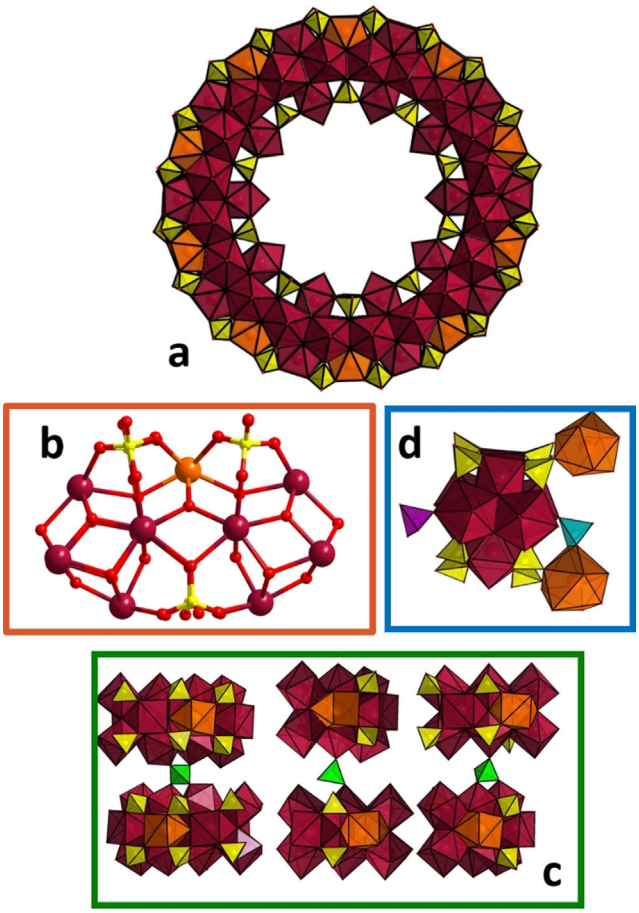

Figure 1. Summary of species that comprise **Ce_{70}-frameworks** a) Polyhedral representation of $[Ce_{70}(OH)_{36}(O)_{64}(SO_4)_{60}(H_2O)_{10}]^{4-}$; the Ce_6 unit is maroon, Ce_1 is orange, sulfate is yellow. b) Ball-and-stick representation of a fragment of Ce_{70}, emphasizing the sulfate bridging between Ce_6 on the inside (towards the bottom) and outside (top) between Ce_1 and a Ce_6. c) Polyhedral representation of addenda sulfates (green) bridging between Ce_{70} rings, based on its connectivity. Left to right: "edge-to-edge", "corner-to-corner", and "edge-to-corner". d) Binding modes of addenda Ce^{IV}-monomers to both Ce_{70}-sulfates and addenda sulfates. Sulfates integral to the Ce_{70}-ring are yellow. The addenda sulfate that chelate a Ce^{IV}-monomers are turquoise, non-bridging addenda sulfates are pink.

prior described U_{70}-family, on the other hand, only displayed the standard offset-stacking arrangement. The Ce-monomer building unit endows the Ce_{70}-family with more diverse supramolecular assembly patterns with pore volumes up to ≈ 60 % free void space (and calculated densities as low as 1.7 g cm^{-3}) exhibited by the tartan and isolated frameworks (Table S12).

Here we consider the effect of reaction conditions and bonding behavior of the TM^{II}-cations on framework assembly. These include TM^{II} concentration, TM^{II} coordination behavior, and solution pH. Metal cation concentration in water and charge-to-size ratio (charge density) mediates pH by hydrolysis, olation and oxalation reactions.[19] Hypothetically, increased aqueous metal concentration and charge-density of the metal cations decrease pH. However, for all reaction solutions with different TM^{II} and different concen-

 © 2021 Wiley-VCH GmbH

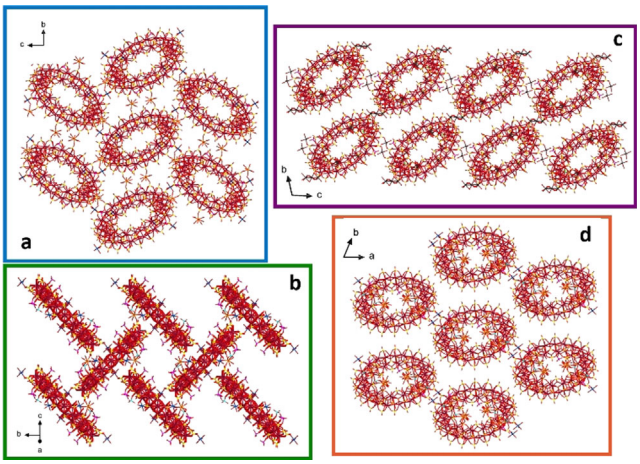

Figure 2. Wireframe representation Ce_{70}-frameworks. a) Propeller framework, b) tartan framework, c) standard offset stacking framework, and d) isolated framework. Ce_{70} is maroon, Ce-monomers are orange, sulfates are yellow, light blue, and pink, TM are dark blue (Co), black (Cd), and oxygens are red.

trations of TM^{II}, the pH before and after heating is 1.5 and 2.5, respectively, suggesting pH has minimal influence on framework assembly. We can therefore assume that in these reaction conditions, the higher valence Ce^{IV} controls acidity, not the divalent transition metals.

One clear correlation is the influence of TM^{II}-concentration on framework arrangement (see synthesis details in the SI). The propeller and offset-stacking frameworks crystallize optimally with $[TM^{II}] = 0.3$ M, the tartan framework crystallizes at $[TM^{II}] = 0.4$ M, and the isolated framework is obtained from at $[TM^{II}] = 0.8$ M. Counterintuitively, increasing the TM^{II} concentration in the reaction solution leads to an increase in Ce-monomer incorporation into the framework (accompanied by decreased TM^{II} incorporation). The extreme case is the isolated framework in which the Ce_{70} rings are completely rimmed and separated by Ce-monomers. We attribute this unexpected trend to the role of the transition metals on the Ce_{70}-formation process. Transition metals could interfere with Ce_{70}-formation, leading to an abundance of Ce-monomers during framework assembly and crystallization. To identify trends in Ce/TM monomer incorporation and their influence on framework type, we have compiled detailed bonding information of these monomers for the reported eight structures (Table S10). Included in this assessment is a parameter summarizing ligation of the monomers by water vs. by sulfate, which describes the collective coordination of the cations. The rich variety of obtained frameworks from specific transition metal, TM^{II}-concentration, and the effect of the incorporated Ce-monomer highlights the complex role of countercations in stabilizing large metal-oxo polyanions, and in the framework assembly thereof. The four different frameworks types are described in detail below, highlighting these roles.

Ce_{70}-Propeller Framework

The "larger" first row TM^{II} at lower concentrations favor the "propeller" framework. **$CoCe_{70}$-propeller**, formulated $CoCe_3Ce_{70}(OH)_{36}(O)_{64}(SO_4)_{65}(H_2O)_{65.5}$ (Table S2), crystallizes in the monoclinic $P2_1/c$, space group ($V = 31298$ Å^3). The structure features offset Ce_{70}-stacking along the *a*-axis, similar to the U_{70} frameworks.[4b,17] The rings are linked by two edge-to-edge sulfates (Figure 1c), four Ce^{IV}-centers apart within the ring. Additional sulfates decorate the ring, charge balancing the Ce- and Co^{II}-monomers. The Ce-monomers direct Ce_{70}-linking in the propeller arrangement via skewed linking (Figure 2a, Figure 3a). Two Ce-monomer sites, related by an inversion center across the ring, bridge one Ce_{70} to two pairs of neighboring Ce_{70} rings on opposite sides of the central ring. These neighboring Ce_{70} rotate $\approx 45°$ from the plane of the central-Ce_{70}, driving the propeller-shaped connectivity (Figure 3a). This Ce-monomer bridges a total of three rings and is 9-coordinate with a tricapped-trigonal prismatic geometry (Figure 3b). Approximately $1/4^{th}$ around the ring is an additional Ce-monomer disordered over two positions (Figure 3c). This monomer bridges the chains approximately along the *b*-axis, reinforcing a three-dimensional framework (Figure S1).Partially occupied octahedral Co^{II}-monomers also participate in framework-linking, either by direct bonding or H-bonding to sulfates through coordinated aqua ligands (Figure S1).

The **$ZnCe_{70}$-propeller** framework (Figure S2a) is analogous to the **$CoCe_{70}$-propeller**, but with decreased ring-connectivity by Zn, similar to the prior U70 respective analogues. Formulated $[Zn(H_2O)_6]Ce_{2.5}Ce_{70}(OH)_{36}(O)_{64}(SO_4)_{64}(H_2O)_{58.5}$ (Table S3), **$ZnCe_{70}$-propeller** crystallizes in the triclinic $P\bar{1}$ space group ($V = 38040$ Å^3). The Zn^{II}-monomers are fully-coordinated by aqua ligands that only interact via H-bonding (Figure S2b). Balancing the loss of Zn^{II}-OSO_3 connectivity, there is an increase in Ce-monomer-sulfate bonding (Table S10).

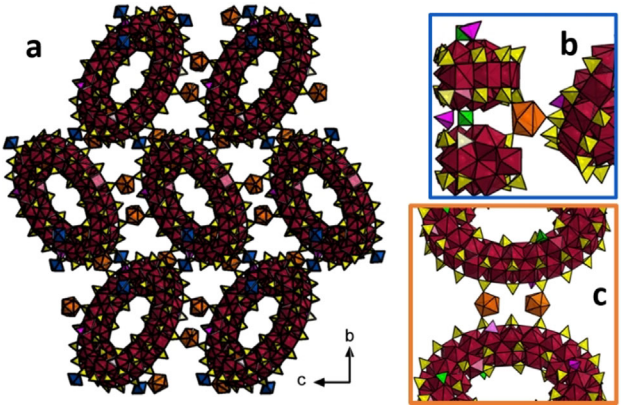

Figure 3. a) Polyhedral representation of **$CoCe_{70}$-propeller**. b) View of Ce-monomer joining three Ce_{70}-rings (oriented top and bottom in (a). c) View of disordered Ce-site joining two rings within the propeller (oriented left and right in (a)). Ce-monomers are orange, Co is blue, addenda sulfates are pink and green.

© 2021 Wiley-VCH GmbH

These are not the final page numbers!

Ce_{70}-Offset-Stacking Framework

The **$NiCe_{70}$-offset-stacking** framework, formulated $Ni_3CeCe_{70}(OH)_{36}(O)_{64}(SO_4)_{63}(H_2O)_{63}$ (Table S4), crystallizes in the triclinic $P\bar{1}$ space group ($V = 16197$ Å^3). An isomorphic Cu-analogue was also obtained, but only the Ni structure will be discussed here. As the main feature of all the U_{70} and Ce_{70} frameworks, the rings are offset stacked along the *a*-axis (Figure 2c). The rings are bridged in the stacking direction by two edge-to-corner sulfates (Figure 1c), five Ce^{IV}-centers apart. The Ce-monomer bridges via a chelating sulfate inside the void of the rings, reinforcing the chain. All Ni^{II}-monomers are 6-coordinate, with four aqua ligands and *trans*-bridging sulfates (Figure S3). The Ni^{II}-monomers bridge chains together, and uniquely bridge rings within the chains (Figure S3b). However, the distorted octahedral geometry of the d^8 Ni^{II} may be viewed as square planar, and not coordinated to the framework. The *trans* Ni-OSO_3 bonds are elongated (2.498–2.521 Å), in comparison to the aqua ligands, Ni—OH_2 1.941–1.997 Å (Table S10).

The **$CdCe_{70}$-offet-stacked** framework, formulated $Cd_7Ce_{70}(OH)_{36}(O)_{64}(SO_4)_{65}(H_2O)_{72}$ (Table S5), crystallizes in the triclinic $P\bar{1}$ space group ($V = 15899$ Å^3). In this framework the ring stacking along the *a*-axis is reinforced by two edge-to-edge sulfates, four Ce^{IV}-centers apart around the ring (Figure S4). The framework features no Ce-monomers, only Cd^{II}-monomers and the corresponding addenda sulfates. The Cd^{II}-monomers are all six-coordinate with four or five aqua ligands, linking rings within and between chains, reinforcing a three-dimensional structure (Figure S4). Interestingly, $CdCe_{70}$ is the only framework that does not contain the Ce-monomer, and this will be important later for confirming redox activity of the frameworks. The Cd^{II} radius is the only TM^{II} that is comparable to Ce (Tables 1 and S10) suggesting the larger radii cations are strong network formers, important in crystallization and subsequent stability.[22]

Ce_{70}-Tartan Framework

$CoCe_{70}$-tartan, formulated $[Co(H_2O)_6]_2Co_2Ce_2Ce_{70}(OH)_{36}(O)_{64}(SO_4)_{66}(H_2O)_{63}$ (Table S6), crystallizes in the monoclinic $P2_1/c$, space group ($V = 34977$ Å^3). This structure does not feature ring-linking sulfates as in the previous structures. Instead, there is an increase in Ce- and Co^{II}-monomer participation in ring-bridging, leading to unique assembly of Ce_{70}. The main structure directing sites is a Ce and a Co monomer (Figure 4a) that bridge neighboring Ce_{70} rings at almost a perpendicular angle (86°), resembling of a tartan pattern (Figure 4b). The remaining Co^{II}-monomers stabilize, and charge balance the structure. Sulfate and water ligated Co interact with neighboring Ce_{70}-rings via H-bonding and direct bonding to sulfate (Figure S5).

$CuCe_{70}$-tartan, fully formulated $CuCe_2Ce_{70}(OH)_{36}(O)_{64}(SO_4)_{62.5}(H_2O)_{61}$ (Table S7), crystallizes in the monoclinic $P2_1/c$ space group ($V = 37328$ Å^3). The structure is roughly similar to $CoCe_{70}$-tartan. Like the Co-analogue, Ce- and Cu^{II}-monomers connect the nearly perpendicular Ce_{70}-rings (89°).

Table 1: Size distribution analysis of SAXS data.

Crystal	TM^{II} ionic radius [Å][b]	Cylinder diameter [Å]	Cylinder height [Å]	Aspect ratio[a]
Dissolved Ce_{70} frameworks				
Offset stack (2-Ce_{70})				
$NiCe_{70}$-offset stacking	0.83	39.7	20.8	0.525
$CuCe_{70}$-tartan	0.87	40.7	21.4	0.525
$ZnCe_{70}$-isolated	0.88	42.6	22.4	0.525
Eclipsed stack (4-Ce_{70})				
$ZnCe_{70}$-propeller	0.88	35.3	61.8	1.75
$CoCe_{70}$-propeller	0.89	33.3	66.6	2
$CdCe_{70}$-offset stacking	1.09	33.3	66.6	2
$CoCe_{70}$-isolated	0.89	34.1	68.2	2
$CoCe_{70}$-tartan	0.89	34.7	69.4	2
Ce_{70} dissolved with added metal cations				
$ZnCe_{70}$-propeller + Ce	1.01 (Ce^{IV})	45.1	23.7	0.525
$ZnCe_{70}$-isolated + Mn	0.97 (Mn^{II})	36.4	72.8	2
$ZnCe_{70}$-isolated + Ca	1.14 (Ca^{II})	36.6	73.2	2
$ZnCe_{70}$-isolated + Ba	1.49 (Ba^{II})	38.4	76.8	2

[a] Aspect ratio = (cylinder height/cylinder diameter). [b] Six-coordinate radius.[22]

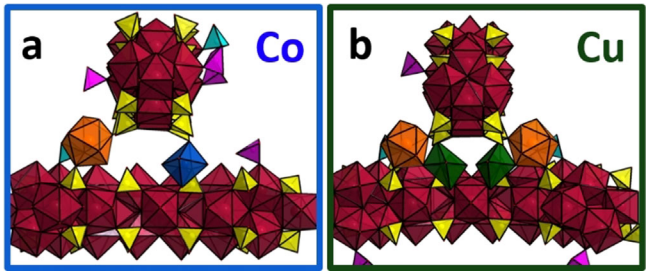

Figure 4. Connectivity of Ce_{70} tartan frameworks. a) Almost perpendicular linking of two Ce_{70} rings in **$CoCe_{70}$-tartan** by a Ce-monomer (orange) and a Co^{II} monomer (blue). b) Similar view of **$CuCe_{70}$**, ring linking via two Cu^{II}-monomers (green) and two Ce-monomers (orange).

Disordered Ce-monomers bridge the perpendicular rings on either side of the Ce_{70} unit (Figure 3e).

Ce_{70}-Isolated Framework

The tendency of Zn to coordinate simply as $[Zn(H_2O)_6]^{2+}$ leads to a new framework type, the isolated framework. Prior-reported X-ray absorption spectra for TM^{II}-sulfates, as well as calculated and empirical stability constants, shows that Zn's full $3d^{10}$ shell, minimizes covalent contributions to bonding with sulfate, meaning sulfate-zinc bonding is less favorable.[23] As aforementioned, we believe the higher TM^{II} concentration slows assembly of Ce_{70} rings, retaining more Ce-monomers as Ce_{70} framework-linkers. Therefore, the isolated-framework topology was also obtained with higher concentration Co^{II}.

© 2021 Wiley-VCH GmbH

The unique aspect of these frameworks is there are no sulfate bridges between the rings, they are only bridged by Ce-monomers, essentially isolating the Ce_{70} rings (Figure 5). **$CoCe_{70}$-isolated**, fully formulated $[Co(H_2O)_6]Ce_{4.5}Ce_{70}(OH)_{36}(O)_{64}(SO_4)_{68}(H_2O)_{65}$ (Table S8), crystallizes in the triclinic $P\bar{1}$ space group ($V = 34915$ Å^3). The lone Co^{II}-monomer site is fully coordinated by aqua ligands and interacts with neighboring chains only via H-bonding (Figure S7). The isostructural **$ZnCe_{70}$-Isolated** framework, formulated $[Zn(H_2O)_6]_{0.5}Ce_{4.5}Ce_{70}(OH)_{36}(O)_{64}(SO_4)_{67.5}(H_2O)_{64.75}$ (Table S9), has a unit cell volume of 39447 Å^3. The sole Zn^{II}-monomer is only half-occupied, limiting interaction in the framework.

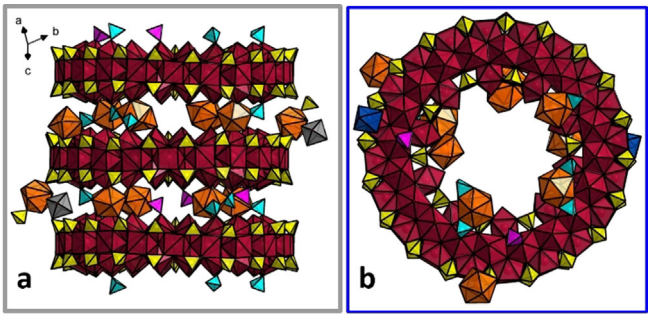

Figure 5. Polyhedral representation of the isolated frameworks. a) Side view of the **$ZnCe_{70}$-isolated** framework showing Ce_{70}-stacking and linking by Ce-monomers, in lieu of ring-bridging sulfates. b) **$CoCe_{70}$-isolated** decorated only by Ce-monomers, along with isolated $Co(H_2O)_6$ octahedra. Ce-monomers are orange, addenda sulfates are pink and turquoise, Co^{II}-monomers are blue, Zn^{II}-monomers are gray.

Supramolecular Assembly in Organic Media

As described for both the Ce_{70} and U_{70} solid-state frameworks, the role of the TM^{II} in the framework assembly depends on the ionic radius and preferred coordination environment.[4b,17] Addenda sulfates also contribute to assembly, arguably the most important U_{70}-linker in the prior described U_{70}-family. In this new Ce_{70}-family, Ce-monomers lead to differentiating assembly, not only in the crystalline lattice, but also in organic media.

TM^{II} counterions play a more significant role in Ce_{70}-linking than they do for U_{70}-linking in organic solvents. Upon dissolution in THF-butylamine, the importance of the architectural building units (TM^{II}, Ce-monomers, ring-bridging sulfates) becomes evident (Figure 6a). All solutions scatter strongly, allowing observation of oscillations, which differentiate varying Ce_{70} arrangements. The dimensions of Ce_{70} is ≈33 Å diameter and ≈4 Å height (Ce-Ce), where the majority of the scattering comes from high-Z Ce (Figure S16).

To determine the size of dissolved Ce_{70}-aggregates, we first performed a size distribution analysis for each scattering curve, using an aspect-ratio cylindrical model (parameters summarized in Table 1, data fitting shown in Figures S11–S14). Two main sizes were observed for the eight reported phases. $NiCe_{70}$-offset stacking, $CuCe_{70}$-tartan, and $ZnCe_{70}$-isolated are a size equivalent to two Ce_{70}-units, offset-stacked (Figure 6c), both based on the dimensions of this dimer, and the similarity to the simulated scattering data (Figure 6a). Notably, this is the dominant solution species observed for all TM^{II}-U_{70} compounds.[4b,17] The remaining five compounds;

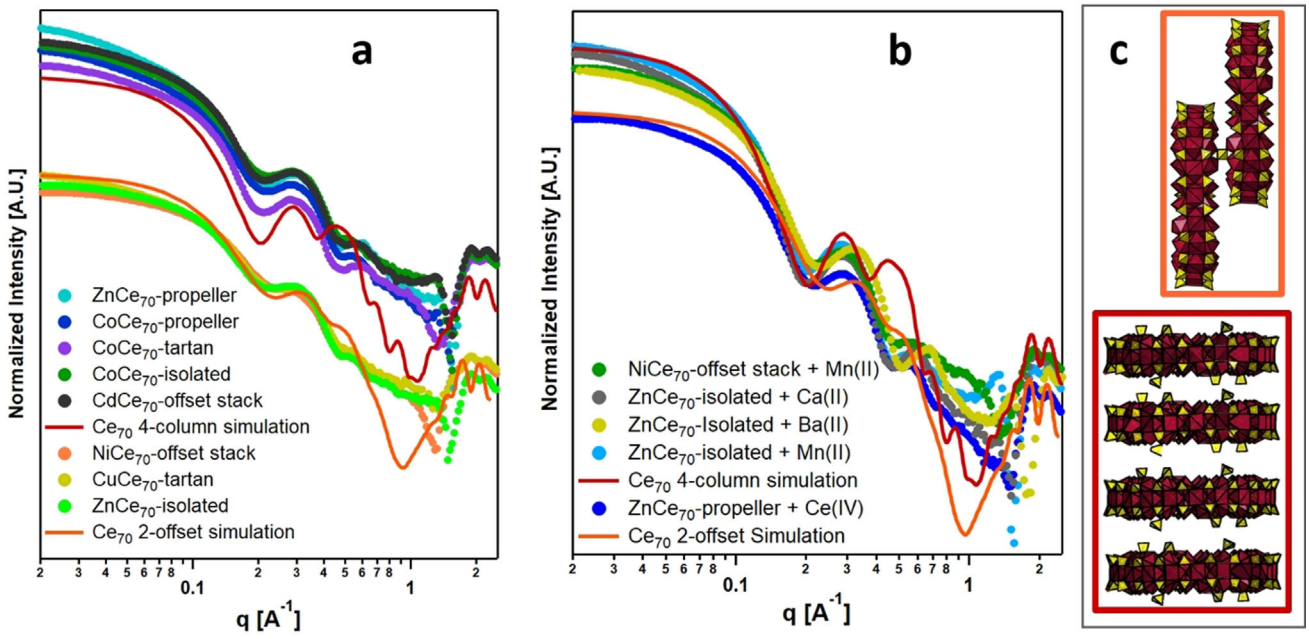

Figure 6. Small angle X-ray scattering of Ce_{70} supramolecular assembly. a) Scattering curves for the eight reported structures, (5.0 mM, dissolved in 3:1 butylamine:tetrahydrofuran solvent mixture). b) Scattering curves for the $ZnCe_{70}$-structures with added Ba^{II}, Ca^{II}, Mn^{II}, and Ce^{IV}, and $NiCe_{70}$ offset-stack with added Mn^{II}. For both plots, scattering curves are vertically-shifted for ease of viewing, and grouped with the simulated curve that they closest match (two Ce_{70} exhibiting offset stacking, or four Ce_{70} exhibiting eclipsed stacking, see ©). c) Polyhedral representation of two Ce_{70}-assemblies, for which scattering is simulated in (a) and (b). The maroon box shows four eclipsed and stacked Ce_{70} (simulated), and the orange box shows an offset dimer, observed in all Ce_{70} frameworks. The box outline matches the color of the simulated scattering curves.

© 2021 Wiley-VCH GmbH

These are not the final page numbers!

three Co-analogues, the $CdCe_{70}$-offset-stack, and the $ZnCe_{70}$-propeller are more consistent with an eclipsed stack of four Ce_{70} rings (Table 1, Figure 6). Differences are noted amongst scattering curves within the two groups that are dominated by one or the other stacking-arrangement (Figure 6a). In particular, there is varying degree of increasing upward slope below $q = 0.1$ Å^{-1}, owed to smaller concentrations of larger aggregates. This is also described by the size distribution data fitting, highlighted in Figure S15.

The eclipsed Ce_{70} 4-stack is unique compared to the prior TM^{II}-U_{70} study. It is tempting to attribute this to linking via the Ce-monomers (the U_{70} phases do not have equivalent monomers), but studies discussed below suggest just the opposite. Moreover, the $CdCe_{70}$ exhibits the eclipsed 4-stack, and it contains no Ce-monomers. In Table 1, the dissolved compounds are organized from smallest to largest observed species, along with TM^{II} ionic radii to enable rationalization of trends. We observe a trend of larger TM^{II} promotes eclipsed stacking, suggesting the transition metals are responsible for linking Ce_{70} together into the eclipsed stack. The $ZnCe_{70}$-isolated and $ZnCe_{70}$-propeller present an interesting case; in the organic media, the former assembles as the offset dimer, and the latter assembles as the eclipsed 4-stack. The stark difference between these two frameworks is the isolated-framework contains more Ce-monomers (see Table S10). To further investigate the role of the Ce-monomers (and other metal cations) on solution-phase assembly, we combined; 1) the $ZnCe_{70}$ isolated framework with Mn^{II}, Ca^{II}, and Ba^{II}, and 2) the $ZnCe_{70}$-propeller framework with Ce^{IV}. The resultant scattering curves are shown in Figure 6b, and the size distribution analysis summarized in Table 1 and Figure S14. Interestingly, addition of Ce^{IV} to the $ZnCe_{70}$-propeller framework led to conversion of the larger eclipsed 4-stack (Figure 6a) to the smaller offset dimer. This suggests that Ce-monomers actually interferes with Ce_{70}-stacking. Based on the many solid-state characterizations of the Ce_{70} and U_{70} frameworks, we know the addenda sulfates play a considerable role in linking M_{70} to transition metals. In addition, these structures evidence the proclivity of sulfate bonding to hard tetravalent metal cations. Therefore, the role of the Ce-monomers in preventing eclipsed stacking might be related to the tendency of these monomers to bind addenda sulfates in solution, preventing sulfate participation in extensive linking of Ce_{70}. In contrast, Mn^{II}, Ca^{II} and Ba^{II} all converted $ZnCe_{70}$-isolated from the offset dimer to the eclipsed 4-stack. In addition to the size-distribution analysis, we performed a core–shell cylinder fit of these latter three scattering curves, to assess if the added metal cation directly links the Ce_{70}-rings into the eclipsed stacks (Figure S9 and Table S14). In the core–shell data analysis, the X-ray scattering length density of the solvent is set at 10×10^{10} cm^{-1} (rho, proportional to the electron density), and the rho-values for the shell (the Ce_{70}-ring stack plus any linking metals) and the core (inside the ring) are refined against the solvent value.[24] Indeed, we observe an increased rho-value from 99 to 110 to 206, for Ce_{70}-shells with added Ca, Mn and Ba, respectively. This is exactly consistent with the increasing number of electrons from 20 to 25 to 56 for Ca, Mn, and Ba, providing compelling evidence that these metals are driving the solution phase connectivity from the offset dimer stack to the eclipsed 4-stack.

Ion Absorption and Oxidation

We probed the cerium redox activity and absorption properties of two representative Ce_{70}-frameworks (by UV-vis of aqueous solutions, before and after contact with Ce_{70}-frameworks; and compositional analysis of the solids, see Table S17, Figures S20–S27).

We found selectivity for metal cations with affinity for binding to sulfate (of the Ce_{70}-rings), and redox activity of the Ce-monomers, not the Ce_{70}-rings. **Cd-Ce_{70}-offset-stacked** and **Zn-Ce_{70}-propeller** have nearly identical void volume ($\approx$45%); the former has no Ce-monomers, the latter has Ce-monomers. In screening studies, the frameworks did not absorb Cs^+ or UO_2^{2+}. However, they absorbed Ln^{3+} and U^{4+}, ions that bind strongly to sulfate: both have large coordination spheres that can include bidentate ligands. We presume the multivalent cations exchange with protons from the acidic, Ce-bond water or H_3O^+ (see formulae, Table S1), since any of the Ce_{70}-frameworks in contact with water decreases its pH to $\approx$2–4. In an initial test, both frameworks absorbed $\approx$3 Nd^{3+} per Ce_{70}-ring (Figure S19), while a titration experiment (Figure 7A) showed absorption of up to six Nd^{3+} per Ce_{70}-ring in **Cd-Ce_{70}-offset-stacked**. Both frameworks absorbed U^{4+} ($\approx$2 U^{4+} per Ce_{70}-ring for **Cd-Ce_{70}-offset-stacked**). UV-vis analysis of the U^{4+}-solution in contact with **Zn-Ce_{70}-propeller** evidences oxidation of U^{4+} to UO_2^{2+} (Figure 7B). This provides two clear conclusions; 1) Ce^{IV}-monomers are redox-active while those that comprise the Ce_{70}-ring are not, and 2) UO_2^{2+} does not readily bind in the Ce_{70}-frameworks. Finally, MnO_4^- sorption was also tested to probe both presence of trivalent Ce-monomers and ion-exchange/sorption of anions (Figure 7C). The **Cd-Ce_{70}-offset-stack** absorbs all the MnO_4^-(approximately one per Ce_{70}-ring), and the mechanism is ion exchange with sulfate. Sulfate's release is evidenced by the rise in intensity below 400 nm. The **Zn-Ce_{70}-propeller** undergoes less anion exchange. However, the rise in background across the visible range is consistent with Mn^{4+} in solution, suggesting the presence of Ce^{III}-monomers. Importantly, these experiments show the Ce-monomers are mixed $Ce^{III/IV}$ (see Table S1), and frameworks containing these can perform both oxidation and reduction.

Conclusion

Molecular cerium oxo-clusters are important for understanding $Ce^{III/IV}$-catalysts, ion conductors and photoabsorbers. In addition, they are surrogates for plutonium analogues. Here we have introduced a new family of Ce^{IV} oxo-clusters, the Ce_{70} wheel is the largest to date, and the only one that does not grow symmetrically about the Ce_6 oxo-cluster core. The $Ce^{IV}{}_{70}$ wheel is analogous to recently reported $U^{IV}{}_{70}$ and $Zr^{IV}{}_{70}$ families, hinting this topology could rival the prolific $M^{IV}{}_6$ and $M^{IV}{}_{38}$ families in ubiquity. Moreover, the insolubility in water and in acid and high pore volumes inspires

 © 2021 Wiley-VCH GmbH

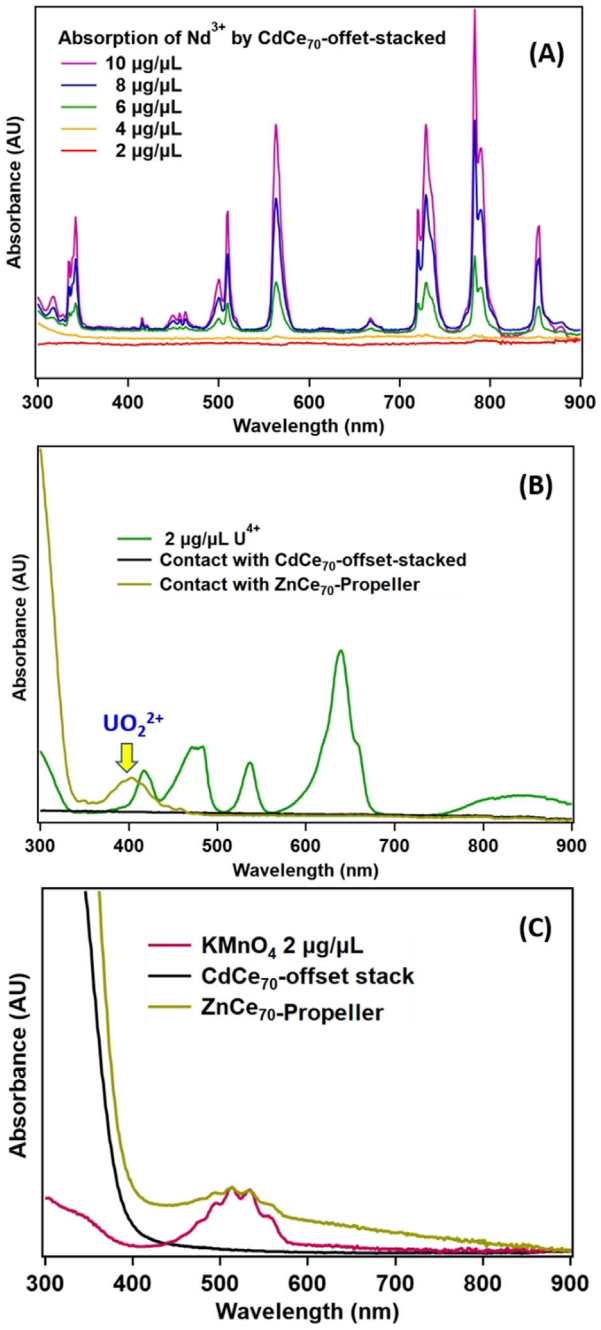

Figure 7. Sorption of ions into **$CdCe_{70}$-offset-stack** (no Ce-monomers) and **$ZnCe_{70}$-propeller** (Ce-monomers) demonstrating cation exchange (a and b) and anion exchange (c), as well as redox activity of Ce-monomers of **$ZnCe_{70}$-propeller**.

exploration of applications in catalysis and molecular sieving, where both selective ion sorption and redox activity (of the monomers) are demonstrated here. Like the U_{70} family, Ce_{70} is isolated readily with TM^{II} countercations. Yet successful utilization of Mg^{2+} and Na^{+} countercations in the Zr_{70} family complicates our understanding of assembly mechanisms, which will also be addressed shortly via isolated intermediates of $Ce^{IV}{}_{70}$. Dissolution of the frameworks in organic media and SAXS analysis reveals the role of lower valence metal cations (i.e. alkaline earths) on promoting supramolecular assembly and higher valence metal cations (i.e. Ce-monomers) on preventing assembly. Thus, in addition to the $M^{IV}{}_{70}$ families crystallized from aqueous media, there is potential to surface-deposit $M^{IV}{}_{70}$-macrostructures from organic media with control over arrangement and connectivity of the rings. In addition to these ongoing efforts, we are translating the $M^{IV}{}_{70}$ chemistry to Pu^{IV}. Outgrowth into these studies represents enormous potential for discovery of both fundamental and applied *f*-block and *d*-block M^{IV} oxo-cluster chemistry.

Acknowledgements

This work was supported by the U.S. Department of Energy, National Nuclear Security Administration (NNSA) under Award Number DE-NA0003763. We acknowledge the Murdock Charitable Trust (Grant No. SR-2017297) for acquisition of the single-crystal X-ray diffractometer.

Conflict of interest

The authors declare no conflict of interest.

Keywords: cerium · polyanions · SAXS · supramolecular chemistry · transition metals

[1] a) M. Amiri, N. P. Martin, O. Sadeghi, M. Nyman, *Inorg. Chem.* **2020**, *59*, 3471–3481; b) W. H. Casey, J. R. Rustad, D. Banerjee, G. Furrer, *J. Nanopart. Res.* **2005**, *7*, 377–387; c) J. M. Fedeyko, D. G. Vlachos, R. F. Lobo, *Langmuir* **2005**, *21*, 5197–5206; d) G. Furrer, B. L. Phillips, K. U. Ulrich, R. Pothig, W. H. Casey, *Science* **2002**, *297*, 2245–2247; e) O. Sadeghi, L. N. Zakharov, M. Nyman, *Science* **2015**, *347*, 1359–1362; f) J. S. Weatherill, K. Morris, P. Bots, T. M. Stawski, A. Janssen, L. Abrahamsen, R. Blackham, S. Shaw, *Environ. Sci. Technol.* **2016**, *50*, 9333–9342; g) H. Xu, S. Sommer, N. L. N. Broge, J. K. Gao, B. B. Iversen, *Chem. Eur. J.* **2019**, *25*, 2051–2058; h) B. Das, *J. Phys. Chem. A* **2018**, *122*, 652–661.

[2] a) B. Chakraborty, I. A. Weinstock, *Coord. Chem. Rev.* **2019**, *382*, 85–102; b) K. Kozma, M. Y. Wang, P. I. Molina, N. P. Martin, Z. Feng, M. Nyman, *Dalton Trans.* **2019**, *48*, 11086–11093; c) L. Soderholm, P. M. Almond, S. Skanthakumar, R. E. Wilson, P. C. Burns, *Angew. Chem. Int. Ed.* **2008**, *47*, 298–302; *Angew. Chem.* **2008**, *120*, 304–308.

[3] a) D. Aulakh, L. M. Liu, J. R. Varghese, H. M. Xie, T. Islamoglu, K. Duell, C. W. Kung, C. E. Hsiung, Y. X. Zhang, R. J. Drout, O. K. Farha, K. R. Dunbar, Y. Han, M. Wriedt, *J. Am. Chem. Soc.* **2019**, *141*, 2997–3005; b) R. Bagai, G. Christou, *Chem. Soc. Rev.* **2009**, *38*, 1011–1026; c) D. Conic, K. Pierloot, T. Parac-Vogt, J. Harvey, *Phys. Chem. Chem. Phys.* **2020**, *22*, 25136; d) Y. Y. Liu, A. J. Howarth, N. A. Vermeulen, S. Y. Moon, J. T. Hupp, O. K. Farha, *Coord. Chem. Rev.* **2017**, *346*, 101–111; e) J. Moons, F. de Azambuja, J. Mihailovic, K. Kozma, K. Smiljanic, M. Amiri, T. C. Velickovic, M. Nyman, T. N. Parac-Vogt, *Angew. Chem. Int. Ed.* **2020**, *59*, 9094–9101; *Angew. Chem.* **2020**, *132*, 9179–9186; f) R. Sessoli, A. K. Powell, *Coord. Chem. Rev.* **2009**, *253*, 2328–2341; g) K. Stroobants, E. Moelants, H. G. T. Ly, P. Proost, K. Bartik, T. N. Parac-Vogt, *Chem. Eur. J.* **2013**, *19*, 2848–2858; h) A. J. Tasiopoulos, A. Vinslava, W. Wernsdorfer, K. A. Abboud, G. Christou, *Angew. Chem. Int. Ed.* **2004**, *43*, 2117–2121; *Angew. Chem.* **2004**, *116*, 2169–2173.

© 2021 Wiley-VCH GmbH

These are not the final page numbers!

[4] a) S. A. Claridge, A. W. Castleman, S. N. Khanna, C. B. Murray, A. Sen, P. S. Weiss, *ACS Nano* **2009**, *3*, 244 – 255; b) I. Colliard, G. Morrison, H. Z. Loye, M. Nyman, *J. Am. Chem. Soc.* **2020**, *142*, 9039 – 9047; c) S. G. Mitchell, C. Streb, H. N. Miras, T. Boyd, D. L. Long, L. Cronin, *Nat. Chem.* **2010**, *2*, 308 – 312; d) F. Xu, H. N. Miras, R. A. Scullion, D. L. Long, J. Thiel, L. Cronin, *Proc. Natl. Acad. Sci. USA* **2012**, *109*, 11609 – 11612; e) G. Y. Zhang, E. Gadot, G. Gan-Or, M. Baranov, T. Tubul, A. Neyman, M. Li, A. Clotet, J. M. Poblet, P. C. Yin, I. A. Weinstock, *J. Am. Chem. Soc.* **2020**, *142*, 7295 – 7300.

[5] a) J. H. Cavka, S. Jakobsen, U. Olsbye, N. Guillou, C. Lamberti, S. Bordiga, K. P. Lillerud, *J. Am. Chem. Soc.* **2008**, *130*, 13850 – 13851; b) C. Falaise, K. Kozma, M. Nyman, *Chem. Eur. J.* **2018**, *24*, 14226 – 14232; c) C. Falaise, H. A. Neal, M. Nyman, *Inorg. Chem.* **2017**, *56*, 6591 – 6598; d) A. Kalaji, L. Soderholm, *Inorg. Chem.* **2014**, *53*, 11252 – 11260; e) K. E. Knope, L. Soderholm, *Inorg. Chem.* **2013**, *52*, 6770 – 6772; f) N. P. Martin, J. Marz, H. Feuchter, S. Duval, P. Roussel, N. Henry, A. Ikeda-Ohno, T. Loiseau, C. Volkringer, *Chem. Commun.* **2018**, *54*, 6979 – 6982; g) R. Das, R. Sarma, J. B. Baruah, *Inorg. Chem. Commun.* **2010**, *13*, 793 – 795.

[6] a) M. Dufaye, S. Duval, G. Stoclet, T. Loiseau, *CrystEngComm* **2020**, *22*, 371 – 380; b) S. Duval, P. Roussel, T. Loiseau, *Inorg. Chem. Commun.* **2017**, *83*, 52 – 54; c) S. Duval, X. Trivelli, P. Roussel, T. Loiseau, *Eur. J. Inorg. Chem.* **2016**, 5373 – 5379; d) S. L. Estes, M. R. Antonio, L. Soderholm, *J. Phys. Chem. C* **2016**, *120*, 5810 – 5818; e) I. L. Malaestean, A. Ellern, S. Baca, P. Kogerler, *Chem. Commun.* **2012**, *48*, 1499 – 1501; f) L. Mathey, M. Paul, C. Coperet, H. Tsurugi, K. Mashima, *Chem. Eur. J.* **2015**, *21*, 13454 – 13461.

[7] S. Jakobsen, D. Gianolio, D. S. Wragg, M. H. Nilsen, H. Emerich, S. Bordiga, C. Lamberti, U. Olsbye, M. Tilset, K. P. Lillerud, *Phys. Rev. B* **2012**, *86*, 125429.

[8] M. Lammert, M. T. Wharmby, S. Smolders, B. Bueken, A. Lieb, K. A. Lomachenko, D. De Vos, N. Stock, *Chem. Commun.* **2015**, *51*, 12578 – 12581.

[9] C. Falaise, J. S. Charles, C. Volkringer, T. Loiseau, *Inorg. Chem.* **2015**, *54*, 2235 – 2242.

[10] C. Falaise, C. Volkringer, J. F. Vigier, N. Henry, A. Beaurain, T. Loiseau, *Chem. Eur. J.* **2013**, *19*, 5324 – 5331.

[11] A. M. Hastings, D. Ray, W. Jeong, L. Gagliardi, O. K. Farha, A. E. Hixon, *J. Am. Chem. Soc.* **2020**, *142*, 9363 – 9371.

[12] K. J. Mitchell, K. A. Abboud, G. Christou, *Nat. Commun.* **2017**, *8*, 0.

[13] C. Falaise, C. Volkringer, J. F. Vigier, A. Beaurain, P. Roussel, P. Rabu, T. Loiseau, *J. Am. Chem. Soc.* **2013**, *135*, 15678 – 15681.

[14] N. P. Martin, C. Volkringer, P. Roussel, J. Marz, C. Hennig, T. Loiseau, A. Ikeda-Ohno, *Chem. Commun.* **2018**, *54*, 10060 – 10063.

[15] a) A. Corma, P. Atienzar, H. Garcia, J. Y. Chane-Ching, *Nat. Mater.* **2004**, *3*, 394 – 397; b) L. D. Fan, C. Y. Wang, M. M. Chen, B. Zhu, *J. Power Sources* **2013**, *234*, 154 – 174; c) J. Paier, C. Penschke, J. Sauer, *Chem. Rev.* **2013**, *113*, 3949 – 3985; d) A. Trovarelli, *Catal. Rev.* **1996**, *38*, 439 – 520.

[16] M. C. Wasson, X. Zhang, K.-i. Otake, A. S. Rosen, S. Alayoglu, M. D. Krzyaniak, Z. Chen, L. R. Redfern, L. Robison, F. A. Son, Y. Chen, T. Islamoglu, J. M. Notestein, R. Q. Snurr, M. R. Wasielewski, O. K. Farha, *Chem. Mater.* **2020**, *32*, 8522 – 8529.

[17] I. Colliard, M. Nyman, *Chem. Eur. J.* **2020**, *26*, 12481 – 12488.

[18] S. Øien-Ødegaard, E. A. R. C. Bazioti, Ø. Prytz, K. P. Lillerud, U. Olsbye, *Angew. Chem. Int. Ed.* **2020**, *59*, 21397 – 21402; *Angew. Chem.* **2020**, *132*, 21581 – 215860.

[19] M. Henry, J. P. Jolivet, J. Livage, *Spectroscopy and Applications of Sol-Gel Glasses*, Springer, Berlin, **1992**, pp. 153 – 206.

[20] a) A. Misra, K. Kozma, C. Streb, M. Nyman, *Angew. Chem. Int. Ed.* **2020**, *59*, 596 – 612; *Angew. Chem.* **2020**, *132*, 606 – 623; b) L. F. Chen, M. J. Turo, M. Gembicky, R. A. Reinicke, A. M. Schimpf, *Angew. Chem. Int. Ed.* **2020**, *59*, 16609 – 16615; *Angew. Chem.* **2020**, *132*, 16752 – 16758; c) H. W. Chen, H. Y. Tu, C. J. Hu, Y. Liu, D. R. Dong, Y. F. Sun, Y. F. Dai, S. L. Wang, H. Qian, Z. Y. Lin, L. W. Chen, *J. Am. Chem. Soc.* **2018**, *140*, 896 – 899; d) L. Bernasconi, E. Fois, A. Selloni, *J. Chem. Phys.* **1999**, *110*, 9048 – 9055.

[21] P. L. Roulhac, G. J. Palenik, *Inorg. Chem.* **2003**, *42*, 118 – 121.

[22] R. D. Shannon, *Acta Crystallogr. Sect. A* **1976**, *32*, 751 – 767.

[23] a) P. Frank, R. K. Szilagyi, V. Gramlich, H. F. Hsu, B. Hedman, K. O. Hodgson, *Inorg. Chem.* **2017**, *56*, 1080 – 1093; b) A. I. Mishustin, *Russ. J. Inorg. Chem.* **2007**, *52*, 283 – 288.

[24] J. Ilavsky, P. R. Jemian, *J. Appl. Crystallogr.* **2009**, *42*, 347 – 353.

Manuscript received: December 12, 2020
Accepted manuscript online: January 7, 2021
Version of record online: ■■ ■■, ■■■■

© 2021 Wiley-VCH GmbH

Research Articles

Oxo Clusters

I. Colliard, M. Nyman* ——— ■■■–■■■

Ce^{IV}_{70} Oxosulfate Rings, Frameworks, Supramolecular Assembly, and Redox Activity

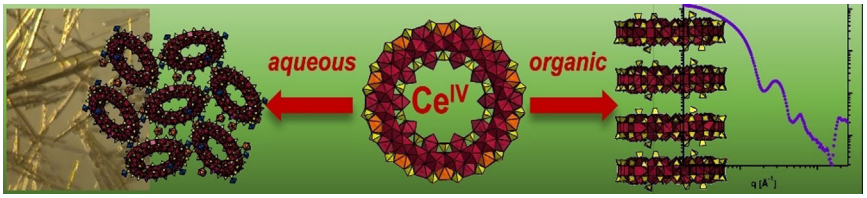

The Ce_{70}-sulfate wheel assembles from water into intricate frameworks with transition metal countercations. Dissolved in organic media, Ce_{70} exhibits very different supramolecular assembly. These frameworks demonstrate redox activity, owed to mixed $Ce^{III/IV}$ linking monomers.

© 2021 Wiley-VCH GmbH

These are not the final page numbers!